Filtering Line Artifacts in Gravitational Waves Using PSO Optimized Piecewise Chirps*

Casey Holman†

Project advisor: Soumya Mohanty‡

Abstract. Gravitational Wave (GW) data is contaminated by many instrumental and environmental artifacts which adversely affect the search sensitivity for astrophysical signals. For the artifacts that cannot be eliminated in hardware, data processing must instead be used to identify and filter them out. Once such artifact is the Wandering Line (WL), a chirp with unpredictable frequency evolution that varies smoothly across a wide frequency band over a sustained period. Due to their large and unpredictable frequency range, WLs are difficult to filter using traditional line removal techniques without risking the removal of astrophysical signals. We propose a novel approach in which the WL is split into smaller segments and Particle Swarm Optimization (PSO) is used to fit a quadratic chirp model that is then subtracted from the data. We test this methodology on simulated WLs generated using random cubic spline frequency functions and added i.i.d. Gaussian white noise. Our results demonstrate that this approach successfully filters simulated WL artifacts with noise that has a standard deviation (s.d.) up to 5 times the WL amplitude. This is more than the noise s.d. to amplitude ratio of 4 we estimate from LIGO data, showing promise for suppressing such artifacts in real GW observations.

1. Introduction.

Detection of Gravitational Waves (GWs) by the Laser Interferometer Gravitation Wave Observatory (LIGO) has allowed for a completely new set of tools with which to investigate astrophysical events. To detect GWs, LIGO measures changes in length with an extreme precision of 10^{-18}m over 4 km, making data collection prone to a variety of undesirable artifacts [1, 13]. The mitigation of these artifacts in turn allows for more accurate study of GWs. If a particular artifact cannot be prevented with engineering, it must instead be identified and eliminated from the output signal. These artifacts are only one part of this noisy composite output signal, but must be accurately modeled despite this. Any inaccuracy can instead alter the other desired signal components when subtracting out the model, thus harming the clarity of GW observations.

This paper will focus on the modeling, and subsequent removal, of one such artifact type known as a Wandering Line (WL) (Fig. 1). WLs are characterized by a continuously varying frequency across a potentially wide band, making them difficult to model with traditional line removal techniques. For example, Median Based Line Tracker is a line filtration method which does not rely on any evolution models and is designed to minimize impact on transients [7]. However, it requires a fixed frequency range that is not feasible for WLs. Coherent Line Removal on the other hand has proven successful at removing unwanted interference in the GW spectrum, even for variable frequency [11]. However, the artifact must be present in several harmonics, which may not be the case in general.

In this paper, we propose a novel approach in which the WL is split into smaller segments

*Funding: This research was supported by NSF grant 2244167

†Department of Physics, Lawrence University, Appleton, WI (casey.s.holman@lawrence.edu).

‡Department of Physics and Astronomy, The University of Texas Rio Grande Valley, Brownsville, TX (soumya.mohanty@utrgv.edu).

Copyright © SIAM

Unauthorized reproduction of this article is prohibited

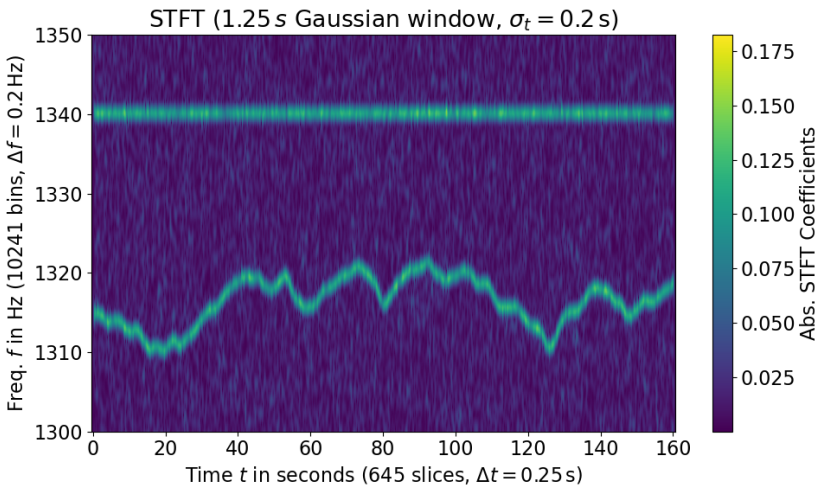

Figure 1. *Bottom half: Spectrogram of a WL artifact from LIGO Hanford strain data H1-1126309928 from GWOSC.org [2]. H1 indicates the 1st Hanford Observatory detector followed by the GPS start time. Top half: Reference sin wave of amplitude 0.25 and constant frequency 1340Hz (See Section V). For the Short-time Fast Fourier Transform (STFT), Δf is the width of frequency bins, Δt is the spacing the STFTs, and σ_t is the standard deviation of the Gaussian weighting used for each window. The strength of each frequency bin at a certain time is shown by the color mapping.*

that are then fit as individual quadratic chirp models using a Particle Swarm Optimization (PSO) algorithm. PSO uses iteratively updated 'particles' that explore the parameter space based on the best individual and group fits [5]. As such, this PSO Optimized Piecewise Chirps model (POPC) allows for a flexible process that can be adapted to the widely varied shapes and frequency ranges seen in WLs. Accuracy for this modeling is tested against increasing levels of artificially added noise to mimic the difficulties of filtering the WL from a noisy composite signal.

All investigations were conducted on simulated artifacts in a Python environment for this preliminary study. Using simulated data allows us to isolate the WL artifact for better performance characterization of the proposed method. Application to real data requires many pre-processing steps that will be pursued in future work due to limitations of our code and computing resources.

The paper is organized as follows. Section 2 covers the creation of the simulated WLs; Section 3 discusses the approximations used with the Least Squares Fit evaluation; Section 4 discusses the PSO algorithm used for fit minimization; Finally, Section 5 discusses the filtration performance with a conclusion following in Section 6.

2. Artifact Generation.

To create simulated WL artifacts, we model the randomly varying frequency evolution by a smooth parametric function

$$x(t;\Omega) = a(t)\cos(\phi(t;\Omega)), \tag{2.1}$$

where t is the time variable, Ω is the set of random-valued parameters, $a(t)$ is the amplitude, and $\phi(t;\Omega)$ is the phase. We chose to model the instantaneous frequency, $f(t;\Omega) = \frac{d}{dt}\phi(t;\Omega)$,

as a cubic spline. For this, we use B-spline functions [3] that generate a 2nd derivative continuous piecewise cubic polynomial function that interpolates N number of 2-dimensional coordinates (Ω) called breakpoints, which act as our model's parameters. Specifically, $\Omega = \{(t_k = kD, f_k)\}$, where $k = 0, 1, \ldots, N-1$ and D is a constant. For this investigation, we used breakpoints with frequency values drawn randomly from a uniform distribution over a user-decided range with mean f_0 and set $D = \frac{10}{f_0}$ (Fig. 2). $f(t;\Omega)$ can then be converted to phase using a numerical integrator, after which independent and identically distributed (i.i.d.) Gaussian noise with standard deviation σ is added to every data point of $x(t)$ to mimic experimental noise. Although the amplitude also varies in time for WLs, $a(t)$ will be fixed to a constant value for this initial study.

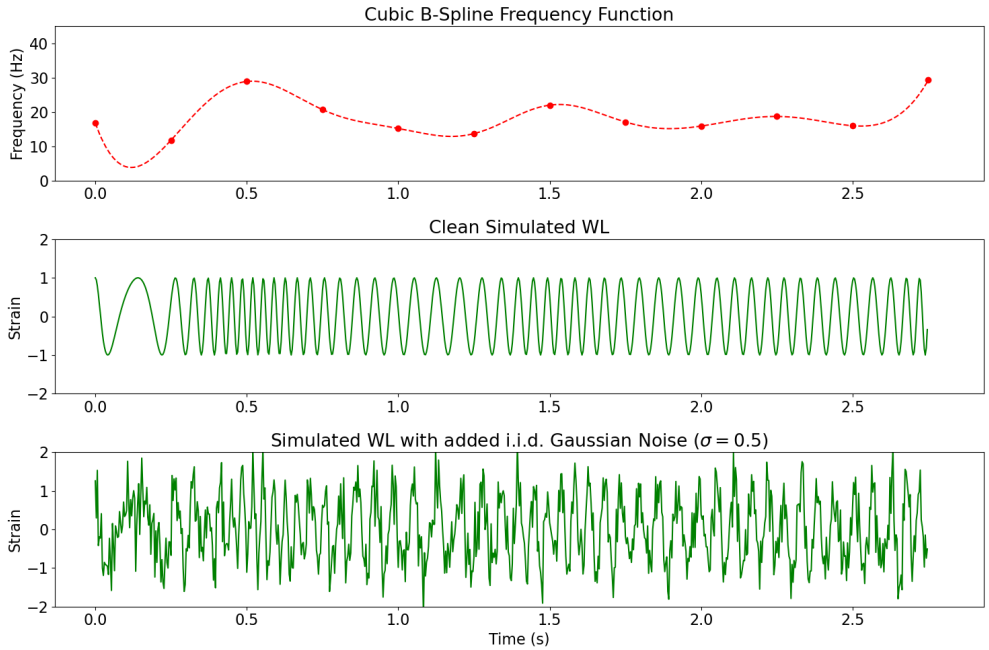

Figure 2. *Top: Example of a simulated WL's frequency domain generated with a quadratic B-Spline function (red dotted line) using randomly generated breakpoints (red dots). Here $f_0 = 20Hz$ and $D = 0.25s$. Middle: The simulated WL artifact generated using the frequency function above. Bottom: The final WL artifact with added i.i.d. Gaussian noise of standard deviation 0.5 times the amplitude.*

3. Fit Evaluation. While the simulated WL is generated using the model given in (2.1), the POPC model we use to fit to the WL is different. This is done to reduce computational costs and the complexity of the optimization problem involved in fitting. First, we assume that if the WL data, x, is broken up into small segments, then the phase for each can be approximated as a degree 3 polynomial. This results in the model

$$S(t;\theta) = a\cos(\phi_0 + \omega_0 t + \omega_1 t^2 + \omega_2 t^3). \tag{3.1}$$

where $\theta = \{a, \phi_0, \omega_0, \omega_1, \omega_2\}$ is our set of parameters. A cubic degree was chosen as a compromise between computational cost and accuracy for this initial study.

We will be using the ordinary Least Squares Function (LSF) to evaluate the fitness of this model. Finding the best fit for each segment then becomes a problem of minimizing the function

$$\sum_i (x_i - S(t_i;\theta))^2 \tag{3.2}$$

over the 5 parameters of θ. However, the best fit values ϕ_0 and a can be minimized analytically given ω_0, ω_1, and ω_2 (Appendix A). As such, we only need to vary those 3 coefficients, greatly reducing computational cost.

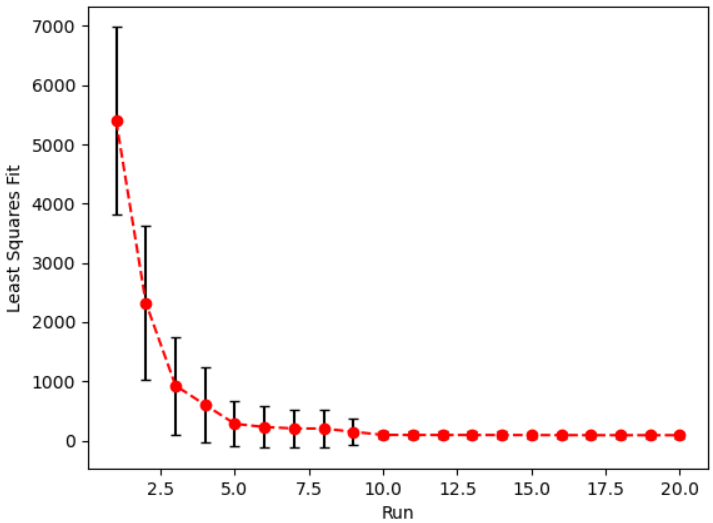

Figure 3. *LSF versus the number of independent PSO runs as averaged over 50 separately fit WL segments. A fixed low i.i.d. Gaussian Noise was used with standard deviation $\frac{1}{5}$ times the amplitude.*

4. Minimization Using PSO. Since the parameters ω_0, ω_1, and ω_2 appear non-linearly, the behavior of the LSF parameter space is extremely difficult to pr edict. Th us, ma ny common minimization algorithms, like Gradient Descent [10], are prone to getting trapped by local minima. Instead, we require an approach that works for a general multi-modal function. We used a type of Swarm Intelligence algorithm well suited for this known as Particle Swam Optimization (PSO) [6]. PSO uses a number of test particles that begin with random coordinates and velocities within the parameter space and move in discrete iterations. Each iteration, a particle's velocity is weighted towards both their previous personal best fit and the entire group's best fit. T his o ften r esults i n a g radual c oncentration o f p articles about a good solution after one particle discovers it, leading to higher resolution in that area and the potential for better solutions [12, 8]. After a preset number of maximum iterations, the parameters that produced the best fit a re r eturned a nd o ne "run" i s c ompleted. T hen, since each run has random starting conditions, better fits can be produced by performing multiple

runs and selecting the best solution from all of them. The mixture of random chance and group behavior is less fine tuned than other minimization methods, but does well at finding the global minimum for a generic search space at low computational cost.

Additionally, we constrained the particles to a limited domain designed to contain the desired minimum. Using Fourier analysis, we can determine the frequency range for each segment, giving $w_0 \in [2\pi f_{min}, 2\pi f_{max}]$. Next, note that for the cubic phase case, the frequency behaves quadratically. Assuming the segment lengths are sufficiently short to justify the quadratic approximation, each segment should contain at most one extremum. Consequently, for a segment duration of Δt, the parameter bounds can be reasonably estimated as $w_1 \in [-\pi \frac{f_{max}-f_{min}}{\Delta t}, \pi \frac{f_{max}-f_{min}}{\Delta t}]$ and $w_2 \in [-\frac{2}{3}\pi \frac{f_{max}-f_{min}}{\Delta t^2}, \frac{2}{3}\pi \frac{f_{max}-f_{min}}{\Delta t^2}]$. While the global minimum may lie outside of this domain, we observed that increasing the search space often led to segment models that failed to transition smoothly between adjacent segments. This is because for POPC an entire WL is modeled as a series of independently fit segments, meaning there is an inherent discontinuity between each. By restricting the domains for all segments, we decrease the likelihood that adjacent segments have substantially different models at the discontinuity, better reflecting the continuous underlying WL behavior in the final reconstructed artifact.

For this investigation we used the `scikit-opt`, an open source Swarm Intelligence package for Python [4]. The number of particles, particle inertia, and the weighting towards group and personal best fits were all chosen from standard values [8]. In order to determine the number of runs to use, we measured the POPC model's best LSF (3.2) for 50 different segments of a simulated WL as a function of runs completed. As the number of runs increases, the chance of finding an even better LSF than in previous runs drops sharply (Fig. 3). This suggests that a run maximum of 10 should produce a good fit without incurring unnecessary computational cost.

Lastly, one additional modification was made to increase fit consistency. We found that occasionally, some segments were difficult to fit accurately when the PSO particles would repeatedly settle on the same poor local minima over many different runs. To remedy this, we split the segment if the model has not achieved an LSF below some predetermined threshold after 10 runs. Each of these half segments are then modeled using the same PSO process. The new half models are only kept if the sum of their LSFs is better than the original model's LSF, otherwise the original model is used. The specific threshold value for this study was chosen heuristically by increasing it until statistically significant outlier LSF segment values dropped to a rate below 5% for a given WL.

5. Results. Within this simulated environment, this POPC methodology showed phenomenally strong filtration results. Three individual examples with increasing noise levels top to bottom can be seen in Fig. 4. At an already high relative i.i.d. Gaussian noise of 2.5 standard deviations per amplitude ($\frac{\sigma}{a}$), POPC is able to consistently and accurately match the underlying frequency function of the simulated WL. After subtraction of this POPC fit, the Power Spectral Density (PSD) peak due to the WL is entirely absent from the residual. As the noise levels increase to $\frac{\sigma}{a} = 5.0$, the spectrogram begins revealing less continuous and occasionally inaccurate models from the POPC fit. For the majority of segments, these issues have a negligible impact on the quality of the model. As a result, the filtration is still largely

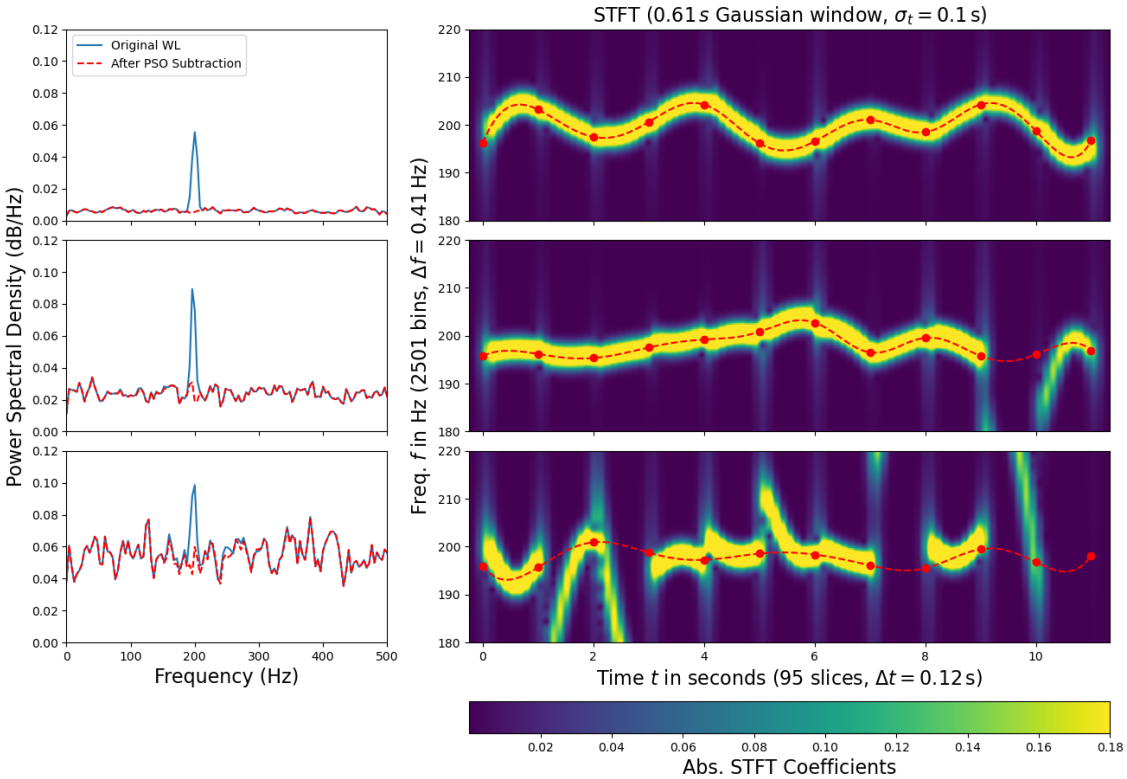

Figure 4. *PSO filtration results of simulated WLs for 3 different noise levels ($\frac{\sigma}{a} = 2.5, 5.0, 7.5$ from top to bottom). The left column shows the Power Spectral Densities before and after the PSO model is subtracted from the WL. The right column shows spectrograms of the PSO models themselves as compared to the underlying frequency function of the WL (red). See Fig. 1 for the spectrogram settings description.*

successful, even if a few segment models have notably poor fits. This decreased performance is not reflected in the PSD as clearly, in part due to the frequency domain restrictions detailed in Section 4. Once the noise begins approaching extremely high levels near $\frac{\sigma}{a} = 7.5$, the model is ineffective, only occasionally matching the underlying artifact's frequency. In the PSD, we can see how the subtraction of this poor fit affects the residual signal outside the frequency range of the original peak.

To compare this performance to a LIGO environment, we can estimate both the standard deviation of background noise and the WL amplitude from strain data H1-1126309928. For WL amplitude, we add a sin wave of constant 1340Hz frequency to the LIGO signal and vary the amplitude until it has a similar spectrogram color mapping to the WL (Fig. 1). This process gives us an estimate of 0.25 for the WL amplitude. For background noise standard deviation, we take a Discrete Fourier Transform (DFT),

$$X_k = \sum_{n=0}^{N-1} x_n \cdot \exp\{-2\pi i \frac{nk}{N}\} \qquad k = 0, \ldots, n-1 \tag{5.1}$$

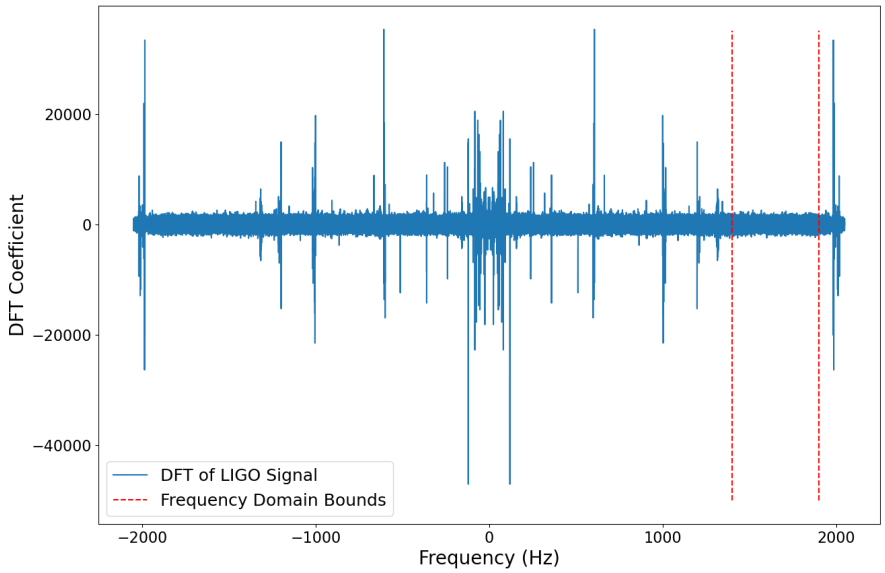

Figure 5. *Discrete Fourier Transform of LIGO Hanford strain data H1-1126309928 from GWOSC.org [2] (See Fig. 1). The selected frequency domain with only background noise is shown in red.*

to convert data in the time domain, x_n, to the frequency domain, X_k (Fig. 5). Now consider Parseval's formula [9],

$$N\sigma^2 \approx \sum_{n=0}^{N-1} x_n^2 = \frac{1}{N} \sum_{k=0}^{N-1} X_k \cdot \overline{X_k}, \tag{5.2}$$

which relates the variance for a function in the frequency and time domains, where σ^2 is average variance of each point in the time domain. Next, we can assume the broadband background noise is uniformly distributed across the frequency range since this LIGO data has already been whitened. If we then isolate a segment in the frequency domain with only background noise (1400-1900Hz), we can use Parseval's formula and correct for the segment's shorter domain with

$$N\sigma^2 \approx \frac{N}{i_2 - i_1} \frac{1}{N} \sum_{k=i_1}^{i_2} X_k \cdot \overline{X_k} \tag{5.3}$$

$$\sigma^2 \approx \frac{1}{i_2 - i_1} \frac{1}{N} \sum_{k=i_1}^{i_2} X_k \cdot \overline{X_k}. \tag{5.4}$$

In doing so, we find a standard deviation of nearly 1 for each point in the time domain, meaning a relative noise standard deviation of approximately 4 for real LIGO data. By comparison,

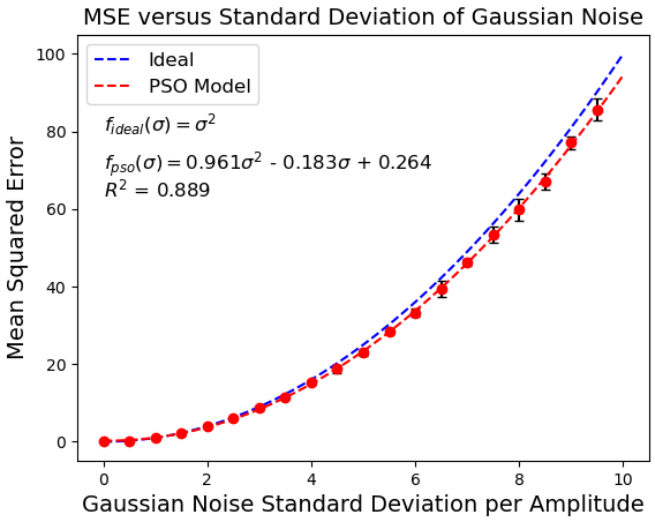

Figure 6. *Mean Squared Error of the PSO model (red) versus the added standard deviation of the i.i.d. Gaussian noise relative to amplitude. An ideal model that leaves only the i.i.d. Gaussian noise is shown in blue.*

the previous qualitative analysis of POPC's performance in the simulated environment showed strong to moderate performance below levels of 5 standard deviations per WL amplitude. This suggests that POPC in its current form could successfully filter LIGO WL artifacts given only this broadband background noise.

The performance can also be evaluated more quantitatively by comparing the Mean Squared Error (MSE) of the POPC model to an ideal model that completely matches the underlying WL. The MSE is given by

$$MSE = \frac{1}{n}\sum_{i=0}^{k}(x_i - S(t_i;\theta))^2. \tag{5.5}$$

If the model is ideal, all that will be left in the residual is the added i.i.d. Gaussian noise. As such,

$$MSE_{ideal} = \frac{1}{k}\sum_{i=0}^{k} N(\mu = 0, \sigma^2)^2 \tag{5.6}$$

$$= \frac{\sigma^2}{k}\sum_{i=0}^{k} Z^2 \sim \frac{\sigma^2}{k}\chi_k^2, \tag{5.7}$$

where $N(\mu, \sigma^2)$ is a normal distribution, Z is the standard normal, and χ_k^2 is the Chi-Squared distribution. The mean of χ_k^2 is simply k, leading to the mean of an ideal model's MSE being just σ^2.

The POPC model was then tested on 10 independent WLs with the MSE averaged across them. This was repeated for a range of fixed noise levels and compared to the ideal model (Fig. 6). POPC still scales approximately with σ^2, but produces MSEs slightly below the ideal case. Thus, the PSO model must be overfitting to the i.i.d. Gaussian noise. For low values of σ, this difference is very small and suggests the model operates near the ideal. As σ increases, this discrepancy gradually widens, indicating that this overfitting worsens at high noise. These results align with the qualitative picture from Fig. 4, strongly suggesting that POPC does negligible damage to the surrounding signal below these extremely high levels of noise.

6. Conclusions. We have outlined a new methodology for removing a type of artifact in LIGO data known as Wandering Lines (WLs). Simulated WLs were created using cubic B-Splines and random breakpoints to mimic their unpredictable frequency variation over time. i.i.d. Gaussian noise is added at the end for better comparison with an experimental setting. The filtration of this artifact then uses a second model, instead approximating small segments of the WL as quadratic chirps. Taking amplitude to be constant, the Least Squares Function (LSF) for each chirp model is shown to be minimized over only 3 parameters, thus reducing complexity. Particle Swarm Optimization (PSO) is then used to minimize the LSF over the non-linear parameter space and produce the model.

This PSO Optimized Piecewise Chirps (POPC) methodology proves to be extremely effective at removing the WL, even up to very noisy artifacts with Gaussian standard deviations of 5 per amplitude. We estimated the actual LIGO broadband background noise standard deviation to be a lower value of 4 times the WL amplitude, supporting the case for POPC's use in real data. Additionally, negligible damage to the surrounding signal is seen at and below these levels of noise in the simulated environment. As the standard deviation of the noise increases further, this POPC model begins substantially overfitting, resulting in worse fit quality and some extraneous damage to the surrounding signal.

One primary limitation of this study is the assumption of constant amplitude in both the POPC model and simulated WLs, which is not the case for real WLs. This limitation is relaxed slightly for the POPC model, since the amplitude is only assumed to be constant over small segments. If the amplitude of a real WL changes slowly enough over time, constant amplitude can be a decent approximation for each individual segment. Another limitation of the model comes from a different approximation made in the parameter reduction. There we treated the sum over time of the chirp model squared as constant with respect to the search parameters. This was observed to cause an underestimation of the PSO model's amplitude resulting in worse quality fits, specifically for WLs with a very slow change in frequency. Due to time constraints this issue was not investigated further, but it may be important to consider for further applications. One final limitation comes from the simplified, simulated data that includes only one white noise source and the WL. In LIGO data the composite signals will have many different components to obfuscate WL filtration. This methodology should be further tested on LIGO data by first bandpassing the WL frequency range to reduce the effect of these other components before fitting.

Overall, POPC works exceedingly well on a wide range of simulated WL data, even for high levels of noise. While limited by simplifying assumptions and synthetic data, the con-

sistent performance of the methodology at levels of noise comparable to LIGO is promising. Future studies may find it beneficial to investigate POPC with different polynomial chirp approximations for potentially stronger results. Going forward, this low cost approach should be explored more extensively to build towards eventual applications to real LIGO data.

Appendix A. Least Squares Fit Parameter Reduction. Let our model be given by $S(t;\theta) := a\,\cos(\lambda(t;\omega))+\phi_0)$ and $\lambda(t;\omega) := \omega_0 t+\omega_1 t^2+...\omega_{n-1}t^n$, where $\theta = \{a, \phi_0, \omega_0, \omega_1, ..., \omega_{n-1}\}$ and $\omega = \{\omega_0, \omega_1, ...\omega_{n-1}\}$. For some dataset $x = \{x_0, x_1, ..., x_k\}$ and $t = \{t_0, t_1, ..., t_k\}$ we can attempt to find the best fit values of θ through minimization of the least squares function,

$$\min_{\theta} \sum_{i=0}^{k} (x_i - S(t_i;\theta))^2. \tag{A.1}$$

If we assume ϕ_0 and a to be dependent on ω, then we can expand and solve the minimizations sequentially with

$$\min_{\omega} \min_{a} \min_{\phi_0} \sum_{i=0}^{k} (x_i - S(t_i;\theta))^2. \tag{A.2}$$

Beginning with ϕ_0,

(A.3)

$$\min_{\phi_0} \sum_{i=0}^{k} (x_i - S(t_i;\theta))^2 = \min_{\phi_0} \sum_{i=0}^{k} (x_i - a\,\cos(\lambda(t_i;\omega) + \phi_0))^2$$

$$= \min_{\phi_0} \sum_{i=0}^{k} (x_i - [a\,\cos(\lambda(t_i;\omega))\,\cos(\phi_0) - a\,\sin(\lambda(t_i;\omega))\,\sin(\phi_0)])^2. \tag{A.4}$$

For simplification, let $\cos(\lambda(t_i;\omega)) = c_i$, $\sin(\lambda(t_i;\omega)) = s_i$, $X = \cos(\phi_0)$, and $Y = \sin(\phi_0)$. If we now minimize over X and Y, an additional constraint must be added to retain the single dimension of ϕ_0, namely $X^2 + Y^2 = 1$. We can then substitute and simplify:

$$= \min_{X,Y} \sum_{i=0}^{k} (x_i^2 + a^2\,c_i^2\,X^2 + a^2\,s_i^2\,Y^2 - 2\,a\,x_i\,c_i\,X + 2\,a\,x_i\,s_i\,Y - 2\,a^2 c_i\,s_i\,X\,Y) \tag{A.5}$$

$$= \sum_{i=0}^{k} x_i + a^2\,N - 2\,a \max_{X,Y} [AX + BY]\,. \tag{A.6}$$

Here we substituted $A = \sum_{i=0}^{k} x_i\,c_i$ and $B = -\sum_{i=0}^{k} x_i\,s_i$ and made a few simplifying approximations. First, that $\sum_{i=0}^{k} \cos(\lambda(t_i))\,\sin(\lambda(t_i)) = \sum_{i=0}^{k} \frac{1}{2}\sin(2\lambda(t_i)) \approx 0$ since the negative and positive values largely cancel out. Second, that $\sum_{i=0}^{k} c_i^2 \approx \sum_{i=0}^{k} s_i^2$, since the $\frac{\pi}{2}$ phase difference makes a negligible difference to the sum. This is only a good approximation for a large number of oscillations over the time series, rendering the phase discrepancy a negligible portion of either sum. As such, we make the substitutions $\sum_{i=0}^{k} c_i^2 = N$ and $\sum_{i=0}^{k} s_i^2 = N$.

From $X^2 + Y^2 = 1$, we know the maximum occurs when

$$X = \cos(\phi_0) = \frac{A}{r} \tag{A.7}$$

$$Y = \sin(\phi_0) = \frac{B}{r}, \tag{A.8}$$

where $r = \sqrt{A^2 + B^2}$. Thus, we can define the best fit ϕ_0 in terms of the ω parameters,

$$\tan(\phi_0) = \frac{B}{A} \Rightarrow \phi_0 = \tan^{-1}(\frac{B}{A}). \tag{A.9}$$

Plugging (A.7) and (A.8) back into (A.6) we find that

$$\min_{\phi_0} \sum_{i=0}^{k} (x_i - a\,\cos(\lambda(t_i;\omega)) + \phi_0)^2 = \sum_{i=0}^{k} x_i + a^2\,N - 2\,ar, \tag{A.10}$$

and can now move onto minimization over a. The three terms form a quadratic, meaning the argmin is $a = \frac{r}{N}$. Thus, we find that the minimization over θ is solely dependent on minimization over ω, namely

$$\min_{\theta} \sum_{i=0}^{k} (x_i - S(t_i;\theta))^2 = \min_{\omega} \left[\sum_{i=0}^{k} x_i - \frac{r^2}{N} \right]. \tag{A.11}$$

Lastly, we can make the approximation that N is constant over different ω values for sampling rates much greater than the maximum frequency given by λ. The final minimization becomes

$$\min_{\theta} \sum_{i=0}^{k} (x_i - S(t_i;\theta))^2 = \sum_{i=0}^{k} x_i - \frac{1}{N} \max_{\omega} \left[r^2 \right]. \tag{A.12}$$

Acknowledgments. I would like to express my gratitude for the continued support and guidance of my mentor Dr. Soumya Mohanty throughout this project. A special thanks to the UTRGV REU faculty and fellow interns who made the time spent in and around this research a truly enjoyable experience. Thanks as well to Thomas Cruz, Alexander Heaton, Leonard Fesemyer, Helin Wang, and Daisy Nguyen for their patient editing and expertise. Lastly, thanks to The University of Texas Rio Grande Valley and The National Science Foundation for funding this work under grant 2244167.

This research has made use of data or software obtained from the Gravitational Wave Open Science Center (gwosc.org), a service of the LIGO Scientific C ollaboration, t he Virgo Collaboration, and KAGRA. This material is based upon work supported by NSF's LIGO Laboratory which is a major facility fully funded by the National Science Foundation, as well as the Science and Technology Facilities Council (STFC) of the United Kingdom, the Max-Planck-Society (MPS), and the State of Niedersachsen/Germany for support of the construction of Advanced LIGO and construction and operation of the GEO600 detector. Additional support for Advanced LIGO was provided by the Australian Research Council. Virgo

is funded, through the European Gravitational Observatory (EGO), by the French Centre National de Recherche Scientifique (CNRS), the Italian Istituto Nazionale di Fisica Nucleare (INFN) and the Dutch Nikhef, with contributions by institutions from Belgium, Germany, Greece, Hungary, Ireland, Japan, Monaco, Poland, Portugal, Spain. KAGRA is supported by Ministry of Education, Culture, Sports, Science and Technology (MEXT), Japan Society for the Promotion of Science (JSPS) in Japan; National Research Foundation (NRF) and Ministry of Science and ICT (MSIT) in Korea; Academia Sinica (AS) and National Science and Technology Council (NSTC) in Taiwan.

REFERENCES

[1] A. Buikema, C. Cahillane, and G. Mansell, *Sensitivity and performance of the advanced ligo detectors in the third observing run*, Physical Review D, 102 (2020), https://doi.org/10.1103/physrevd.102.062003, http://dx.doi.org/10.1103/PhysRevD.102.062003.

[2] T. L. S. Collaboration, the Virgo Collaboration, and the KAGRA Collaboration, *Open data from ligo, virgo, and kagra through the first part of the fourth observing run*, 2025, https://arxiv.org/abs/2508.18079, https://arxiv.org/abs/2508.18079.

[3] C. De Boor and C. De Boor, *A practical guide to splines*, vol. 27, springer New York, 1978.

[4] G. Fei, *scikit-opt*. https://github.com/guofei9987/scikit-opt/, June 2021.

[5] J. Kennedy and R. Eberhart, *Particle swarm optimization*, in Proceedings of ICNN'95 - International Conference on Neural Networks, vol. 4, 1995, pp. 1942–1948 vol.4, https://doi.org/10.1109/ICNN.1995.488968.

[6] J. Kennedy and R. Eberhart, *Particle swarm optimization*, in Proceedings of ICNN'95 - International Conference on Neural Networks, vol. 4, 1995, pp. 1942–1948 vol.4, https://doi.org/10.1109/ICNN.1995.488968.

[7] S. D. Mohanty, *Median based line tracker (MBLT): Model independent and transient preserving line removal from interferometric data*, Class. Quant. Grav., 19 (2002), pp. 1513–1519, https://doi.org/10.1088/0264-9381/19/7/338.

[8] S. D. Mohanty, *Swarm Intelligence Methods For Statistical Regression*, Taylor and Francis Group, 2019.

[9] M.-A. Parseval, *Mémoire sur les séries et sur l'intégration complète d'une équation aux différences partielles linéaire du second ordre, à coefficients constants*, Mémoires présentés à l'Institut des Sciences, Lettres et Arts, par divers savants, et lus dans ses assemblées. Sciences, mathématiques et physiques. (Savants étrangers.), 1 (1806).

[10] S. Ruder, *An overview of gradient descent optimization algorithms*, 2017, https://arxiv.org/abs/1609.04747, https://arxiv.org/abs/1609.04747.

[11] A. M. Sintes and B. F. Schutz, *Coherent line removal: Filtering out harmonically related line interference from experimental data, with application to gravitational wave detectors*, Phys. Rev. D, 58 (1998), p. 122003, https://doi.org/10.1103/PhysRevD.58.122003, https://link.aps.org/doi/10.1103/PhysRevD.58.122003.

[12] A. Tam, *A gentle introduction to particle swarm optimization*. https://machinelearningmastery.com/a-gentle-introduction-to-particle-swarm-optimization/, October 2021.

[13] V. Tiwari, M. Drago, V. Frolov, S. Klimenko, G. Mitselmakher, V. Necula, G. Prodi, V. Re, F. Salemi, G. Vedovato, and I. Yakushin, *Regression of environmental noise in ligo data*, Classical and Quantum Gravity, 32 (2015), p. 165014, https://doi.org/10.1088/0264-9381/32/16/165014, http://dx.doi.org/10.1088/0264-9381/32/16/165014.